Available online at www.sciencedirect.com
SCIENCE DIRECT
International Journal of Solids and Structures 43 (2006) 3527–3541
INTERNATIONAL JOURNAL OF SOLIDS and STRUCTURES
www.elsevier.com/locate/ijsolstr

Effect of heating-rate on the thermomechanical behavior of aluminum alloy LY12 and a phenomenological description ☆

X. Peng *, X. Zhang, J. Fan, B. Chen

Department of Engineering Mechanics, Chongqing University, Chongqing 400044, China

Received 1 March 2005; received in revised form 10 August 2005
Available online 19 December 2005

Abstract

The effect of heating-rate and its history on the thermomechanical behavior of aluminum alloy LY12 is investigated with a Gleeble 1500 thermal–mechanical material testing system. It was found that the material experiencing higher heating-rate histories possesses lower rupture strength, and the pre-stressed material fails at a lower temperature when it is heated at a higher heating-rate. The SEM observation shows that, in general, there are more defects in the material subjected to higher heating-rates or higher heating-rate histories. The concept of local thermal inconsistency is introduced to account for the effect of heating-rate on mechanical properties, such as hardening and damage. A constitutive model is proposed for the description of the behavior of the materials subjected to thermomechanical loading incorporating fast heating, which can take into account the effect of plastic deformation, temperature and its rate, and recrystallization on the mechanical property, hardening and damage of the material. The constitutive behavior of LY12 subjected to uniaxial thermomechanical loading incorporating fast heating is described, and the comparison with the experimental results demonstrates the validity of the proposed model.

Keywords: Aluminum alloy; Heating-rate; Thermomechanical properties; Damage; Constitutive model

1. Introduction

The failure of materials and structures caused by the deposition of highly concentrated energy is receiving increasing attention (Chen et al., 1992, 1995; Chen and Li, 1992; Li and Chen, 1994; Chen, 1997; Liu et al., 1995, 1996; Wang et al., 1995; Han et al., 1999; Peng et al., 2003). A significant phenomenon is that the high and rapid increasing temperature may result in remarkable changes in the mechanical properties as well as the microstructure of materials. It may cause the failure of a preloaded structure due to the degradation of the mechanical properties (e.g., the strength is reduced to below the applied stress), or the invalidation of the designed functions due to redistribution of stress or intolerant changes of configuration. The study of

☆ Financially supported by NSFC (19272119) and the Ministry of Education of China.
* Corresponding author. Fax: +86 23 6510 6656.
E-mail address: xhpeng@cqu.edu.cn (X. Peng).

0020-7683/$ - see front matter © 2005 Elsevier Ltd. All rights reserved.
doi:10.1016/j.ijsolstr.2005.10.002

the material degradation at high and rapid increasing temperature may, on one hand, help avoiding such kind of failure, and on the other hand, provide available information for making use of fast-heating technology. The effect of elevated temperature on the mechanical properties of materials has been studied extensively, but less attention has been paid to the effect of heating-rate.

It was found that fast heating could cause distinct changes in the mechanical properties of aluminum alloy LY12 (Liu et al., 1995; Wang et al., 1995). When investigating the non-linear softening of aluminum alloy and brass subjected to fast heating, it was found that different heating-rate histories may result in differences in both the grain size and the macroscopic mechanical properties, which was accounted for with the dynamics of recrystallization (Liu et al., 1995). The tensile testing of low-alloy steel 30CrMnSi subjected to fast heating histories with different heating-rates showed distinct difference in both the rupture strength and the metallograph of the material (Wang et al., 1995). The experimental investigation to the effect of heating-rate on the mechanical properties of preloaded brass H62 indicated that the failure temperature is reduced with the increase of heating-rate, which was attributed to the increase of microdefects due to strong local thermal inconsistency (LTI) at high heating-rate (Chen et al., 2001). An experiment was conducted to investigate the effect of heating-rate history on the rupture strength of aluminum alloy LY12, and the effect of heating-rate on the failure temperature of pre-loaded LY12 specimens, which confirmed the degradation of the mechanical properties of the material at high heating-rates (Peng et al., 2003). A numerical simulation, which is based on the inhomogeneous nature of the material, showed marked additional stress at high heating-rates, indicating that, at a high heating-rate, LTI may play an important role in the damage and failure of the material (Peng et al., 2003).

In the work reported in this paper, the effects of heating-rate and its history on the mechanical properties of aluminum alloy LY12 are experimentally investigated with a Gleeble 1500 thermal–mechanical material testing system. The microstructure of the tested material is observed with an Amray KYKY-1000B SEM to investigate the mechanisms of the heating-rate effect. It is found that high heating-rate may cause marked changes in both the mechanical properties and the microstructure of the material. It involves temperature-induced softening, hardening, damage, phase transformation, recrystallization, grain growth, etc., and their interactions. A phenomenological model is proposed, taking into account temperature induced variation of material properties, hardening and damage induced by both plastic deformation and LTI, recovery of hardening due to recrystallization. The effect of heating-rate and its history on the thermomechanical behavior of LY12 is described. The satisfactory agreement between the experimental and computed results demonstrates the validity of the proposed model.

2. Experiment

Three classes of experiments are performed with a Gleeble 1500 thermal–mechanical material testing system. The specimens are heated by applying a direct electrical voltage drop between their two ends. The temperature is measured with a chromel–alumel thermocouple welded directly on the surface of the working section and controlled with a computer. The prescribed heating-rate can be realized through the variation of temperature against time. The elongation of a specimen, the tensile traction and the temperature are recorded synchronously with the data acquisition element of the testing system. The material used is aluminum alloy LY12 at age-hardening state (corresponding to aluminum alloy 2024 in USA), with the composition listed in Table 1. The solidus and the melting temperatures of LY12 are about 530 °C and 650 °C, respectively. The geometry of the specimen is shown in Fig. 1, where a reedy working section is used for larger electric resistance to meet the requirement of high heating-rate and a uniform distribution of temperature in the working section. The finite element simulation for the temperature in the aluminum specimen generated by different electrical voltage drops shows sufficiently uniform distributions of the temperature in the working section

Table 1
Composition of the aluminum alloy LY12 (%)

Cu	Mg	Mn	Fe	Si	Al
4.59	1.54	0.75	0.32	0.33	Rest

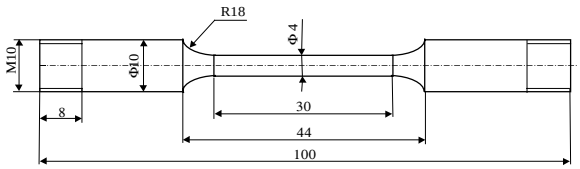

Fig. 1. Geometry of specimen.

of the specimen during the working intervals, provided the diameter of the working section keeps uniform. Three specimens are used for each testing condition, and the results shown below is their average.

In the first class of experiment, the effect of heating-rate history on the rupture strength σ_f of LY12 is investigated. It includes three steps: heating a specimen at a constant heating-rate to a prescribed temperature; keeping the temperature unchanged for 0.5 s, followed by stretching the specimen until fracture. The strain rate is fixed as $0.5\ s^{-1}$, so that the total time interval of this step is less than 0.1 s.

Three final working temperatures, 210, 350 and 465 °C (483, 623 and 738 K), are prescribed and three heating-rates 200, 650 and 1100 K/s are adopted for each working temperature, respectively. The maximum working temperature is less than solidus temperature. The maximum heating-rate is limited by the capability of the testing system, the geometry of specimen and the properties of the used material. Some experimental T–t (temperature vs. time) curves are shown in Fig. 2, where the maximum temperature is prescribed as 465 °C. It can be seen that during heating processes, the slope of the curves is satisfactorily linear, indicating the heating-rate is almost constant. The average heating rates calculated from the curves are shown in the figure, which shows satisfactory agreement with the prescribed ones.

The rupture strength σ_f against heating-rate at different temperatures is shown in Fig. 3. It can be seen that, in general, σ_f decreases with the increase of heating-rate. But at $T = 350$ °C (623 K) σ_f slightly increases as heating-rate increases, which can be accounted for with the concept of LTI (Peng et al., 2003). At lower temperature, the hardening induced by LTI may be less significant compared with the inelastic deformation induced damage. At $T = 350$ °C the hardening induced by LTI becomes prominent, because the rapid recrystallization at this temperature may eliminate some microdefects and increase the deformability of the material. At $T = 465$ °C, the damage induced by LTI may becomes dominant again because of the growth of grain and the temperature induced softening of the material may counteract the effect of hardening and the improvement induced by recrystallization.

The second class of experiment is also to investigate the effect of heating-rate history on σ_f of LY12. It includes the following steps: heating a specimen at a constant heating-rate to the prescribed temperature, keeping the temperature unchanged for 0.5 s and then cooling freely to room temperature, followed by stretching the specimen until fracture. Two maximum temperatures, 210 and 350 °C (483 and 623 K), are prescribed and three heating-rates 200, 650 and 1100 K/s are adopted for each, respectively. Fig. 4 shows the effect of heating-rate on

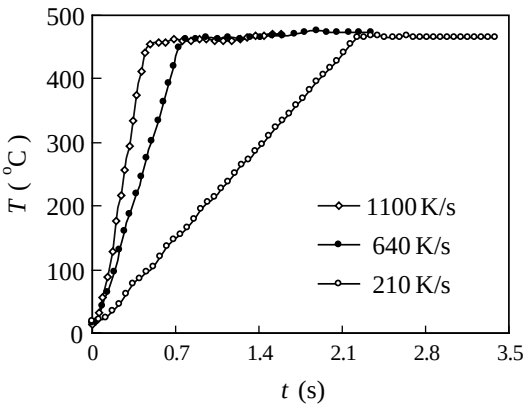

Fig. 2. Experimental T–t curves.

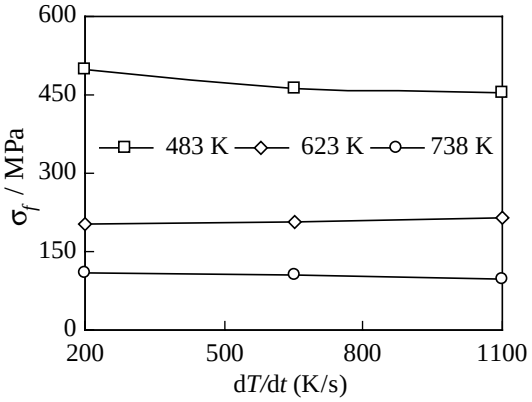

Fig. 3. The effect of heating-rate on σ_f (tension at elevated temperature).

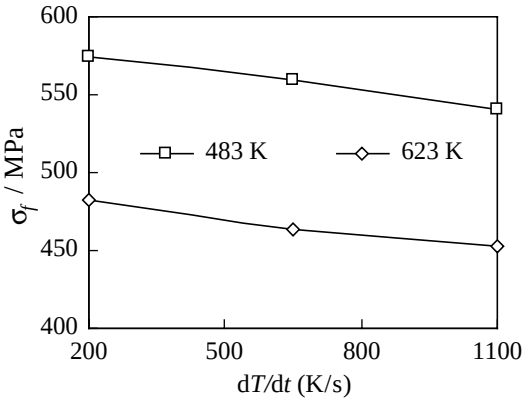

Fig. 4. The effect of heating-rate on σ_f (tension at cooled state).

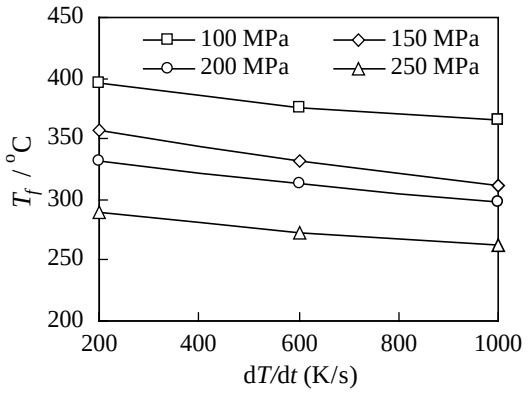

Fig. 5. Variation of failure temperature against heating rate.

σ_f, where it can be seen that the material subjected to the history of higher heating-rate has lower rupture strength. Besides, the history of higher temperature also results in a reduction of σ_f, which may be attributed to the temperature induced softening, recrystallization or the change in the microstructure of the material.

In the third class of experiment, the effect of heating-rate on the failure temperature T_f of preloaded LY12 specimens is to be investigated. It contains two steps: (1) stretching a specimen to a prescribed tensile stress;

and (2) keeping the preloaded stress unchanged and heating the specimen at a prescribed heating-rate until fracture. It could be imagined that, with the increase of temperature, the specimen might gradually lose the capability of bearing the preloaded stress because of softening at elevated temperature. The failure temperature should, therefore, be defined as the temperature at which the prescribed preloaded stress can no longer be held (or falls distinctly), i.e., the specimen loses the capability of bearing the prescribed preloaded stress. Four levels of preloaded stress, 100, 150, 200 and 250 MPa, are prescribed, for each of which three different heating-rates, 200, 600 and 1000 K/s, are assigned. The variation of the failure temperature, T_f, of specimens subjected to different levels of preloaded stress against heating-rate is shown in Fig. 5, where it can be seen that, in general, the increase of either preloaded stress or heating-rate may reduce the failure temperature.

3. SEM observation and analysis

It is known that, when subjected to thermomechanical loading, the change of the mechanical properties of a material is closely related to the microstructure of the material and its variation. For example, dislocation substructure, damage, phase transformation, recrystallization, growth of grains, etc., may strongly influence the mechanical properties as well as the failure mode of the material. In order to make clear the mechanisms of the effect of heating-rate and its history on the mechanical properties of LY12, the metallographs of the fracture surfaces are observed with a SEM and analyzed.

The SEM metallographs of the fracture surfaces of the tested specimens subjected to different heating-rate histories are shown in Fig. 6. Fig. 6(a) and (c) correspond respectively to the specimens heated at $\dot{T} = 200$ K/s to 210 °C and 465 °C followed by tension until fracture, and Fig. 6(b) and (d) correspond respectively to the specimens heated at $\dot{T} = 1100$ K/s to 210 °C and 465 °C and then stretched until fracture. Comparison shows that heating-rate strongly affects the morphology of the fracture sections: at lower heating-rate, the fracture is mostly ductile; while at a higher heating-rate, the fracture is more brittle. On the other hand, it can be seen that the fracture surfaces corresponding to the lower heating-rate are dimply and mostly ductile, and those corresponding to the higher heating-rate look more brittle and contain more defects.

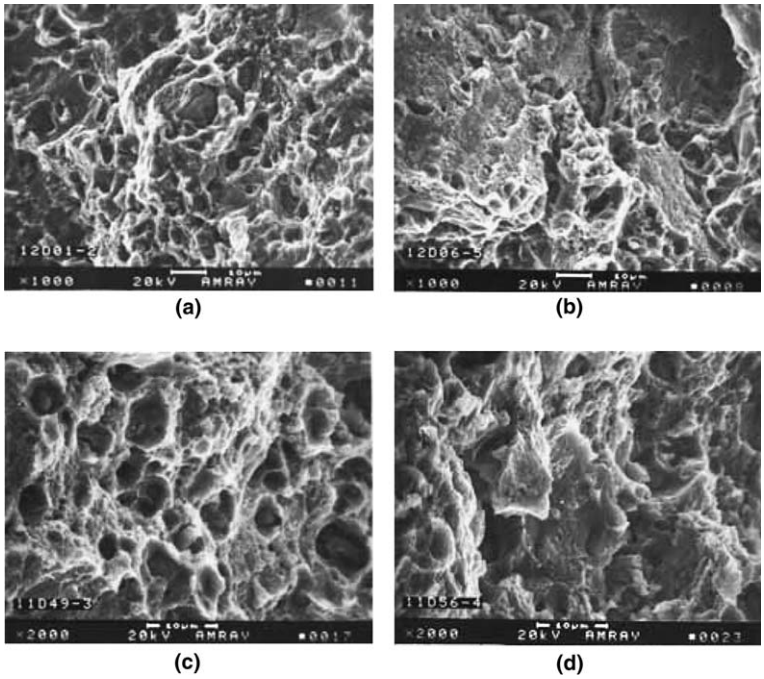

Fig. 6. Metallographs of fracture surfaces of tensile specimens subjected to different heating-rate histories (a) $T = 210$ °C, $\dot{T} = 200$ °C/s (×1000), (b) $T = 210$ °C, $\dot{T} = 1100$ °C/s (×1000), (c) $T = 465$ °C, $\dot{T} = 200$ °C/s (×2000) and (d) $T = 465$ °C, $\dot{T} = 1100$°C/s (×2000).

Fig. 7 shows the SEM metallographs of the fracture surfaces of the tested specimens subjected to preloaded stress $\sigma_0 = 250$ MPa and heated at different heating-rates. Fig. 7(a) corresponds to $\dot{T} = 200$ K/s, where dimpled morphology can be observed, indicating fracture is mainly ductile. The metallographs shown in Fig. 7(b) correspond to the test with $\sigma_0 = 250$ MPa and $\dot{T} = 1000$ K/s, where it can be seen that the fracture is more brittle with more defects.

Comparing the results shown in Fig. 3 through Fig. 7, it can be seen that heating-rate plays a significant role in both the macroscopic behavior and the microstructure of the material. In general, higher heating-rate results in severer degradation of the mechanical properties of the material and more microdefects in the material.

In order to provide more microstructural information for the establishment of the corresponding constitutive model, it is worthwhile to repeat some remarks related to the observation of the microstructure with a light microscope (Peng et al., 2003). The observation near the fracture portion of the tensile specimens subjected to different heating-rate histories shows that, for a fixed working temperature T_f, more defects can be found in the specimens undergoing higher heating-rate histories. The observation near the fracture portion of the tensile specimens, which were preloaded to different level of stress and then heated at different heating-rate until fracture, shows that, with the increase of heating-rate, microdefects increase in both density and size. On the other hand, distinct recrystallization can be observed in the specimen subjected to higher preloaded stress and heated with lower heating-rate (or longer heating time interval).

The effect of heating-rate on the mechanical properties of the material can be accounted for with the concept of local thermal inconsistency (LTI). It is known that most engineering materials are, in nature, heterogeneous. The inhomogeneous nature of the microstructure, such as heterogeneity, grains with different orientations, grain boundaries and phase boundaries, dislocations and dislocation substructures, inclusions, etc., may give rise to the difference in the physical, thermal and mechanical properties in different material elements. It may cause LTI, i.e., non-uniform distribution of local temperature, as well as local residual stress distribution during a fast heating process. For example, when a material is heated with large electrical current, the difference in the electrical and thermal properties between local elements may result in a non-uniform distribution of local temperature. It, in turn, results in additional local residual stress, besides the conventional macroscopic residual thermal stress (Peng et al., 2003). Moderate local residual stress may cause hardening,

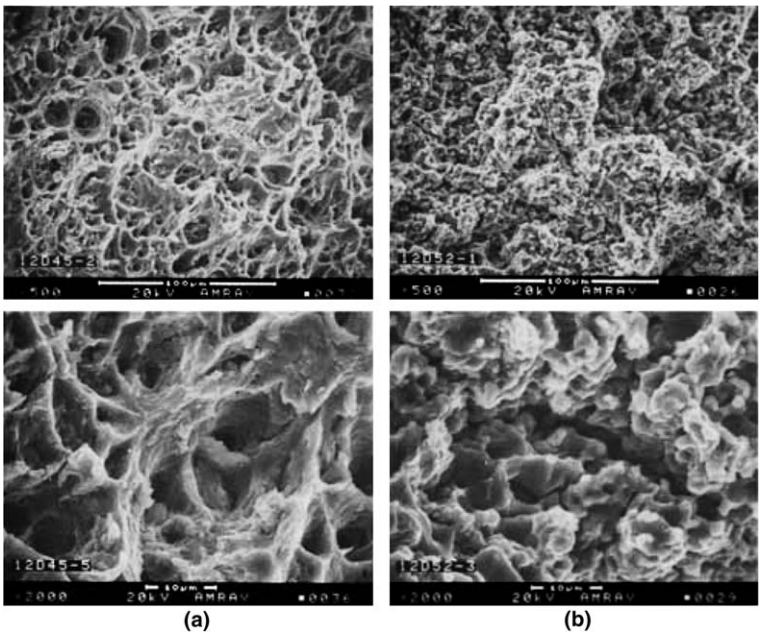

Fig. 7. SEM metallographs of fracture surfaces of tensile specimens subjected to different preloaded stress and heated at different heating-rates (a) $\sigma_0 = 250$ MPa, $\dot{T} = 200$ K/s (b) $\sigma_0 = 250$ MPa, $\dot{T} = 1000$ K/s.

contributing to an improvement of the mechanical property. At a sufficiently large heating-rate, the induced severe LTI may result in very high local temperature and local residual stress. The former may induce local softening, and the latter may cause local damage, which may degrade the mechanical properties of material and make the material fail even at a low level of preloaded stress.

4. Constitutive model

4.1. Constitutive formulation

In a series of papers (Fan and Peng, 1991; Peng and Ponter, 1994; Peng et al., 1997) a thermomechanically consistent constitutive formulation was proposed for dissipative materials, based on a simple mechanical model. Assuming the material to be initially homogeneous and isotropic, the inelastic behavior can be represented with the model shown in Fig. 8. It consists of n Maxwell-type models arranged in parallel together with one spring element in series. The elastic response of a material is represented with the spring E (with macroscopic elastic shear modulus $\bar{G}$ and the inelastic response by the various parallel elements. The rth dissipative mechanism is described with the spring C_r (with stiffness $\bar{C}_r$) and the dashpot-like block a_r (with plastic damping coefficient $\bar{a}_r$). The energy stored in C_r during an inelastic deformation process corresponds to that stored in the microstress fields determined by the respective pattern of defects at microlevels, such as distortion of lattices and dislocations, etc. In the case of small deformation, one has

$$\mathbf{s} = \sum_{r=1}^{n} \mathbf{Q}^{(r)} \tag{1}$$

$$\mathbf{Q}^{(r)} = \bar{C}_r(\mathbf{e}^{\mathrm{i}} - \mathbf{p}^{(r)}) \tag{2}$$

with

$$\mathbf{e}^{\mathrm{i}} = \mathbf{e} - \mathbf{e}^{\mathrm{e}}, \qquad \mathbf{e}^{\mathrm{e}} = (2\bar{\mu})^{-1} : \mathbf{s}, \tag{3}$$

where $\mathbf{e}^{\mathrm{i}}$, $\mathbf{e}^{\mathrm{e}}$ and $\mathbf{e}$ represent inelastic, elastic and total deviatoric strain tensors, respectively; $\mathbf{s}$ is the deviatoric stress tensor, $\mathbf{p}^{(r)}$ and $\mathbf{Q}^{(r)}$ are respectively the rth deviatoric internal variable and the corresponding generalized force, which satisfy the following dissipation inequality:

$$\mathbf{Q}^{(r)} : \mathrm{d}\mathbf{p}^{(r)} \geqslant 0 \quad (r = 0, 1, \ldots, n). \tag{4}$$

$\mathbf{Q}^{(r)}$ is assumed to relate the generalized rate of $\mathbf{p}^{(r)}$ through $\bar{a}_r$ by the following simple relationship:

$$\mathbf{Q}^{(r)} = \bar{a}_r \frac{\mathrm{d}\mathbf{p}^{(r)}}{\mathrm{d}\zeta}, \tag{5}$$

where $\mathrm{d}\zeta$ can be defined in terms of the distance between two adjacent states of inelastic strain as

$$\mathrm{d}\zeta^2 = \mathrm{d}\mathbf{e}^{\mathrm{i}} : \mathrm{d}\mathbf{e}^{\mathrm{i}} \tag{6}$$

and ζ can be regarded as a generalized time measure.

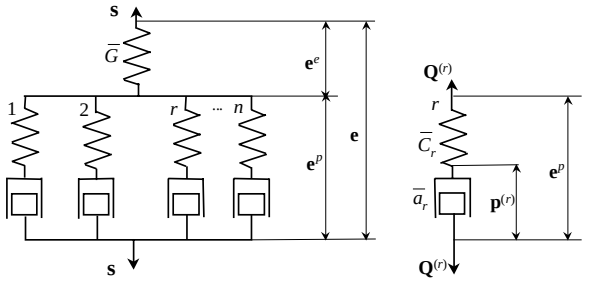

Fig. 8. A simple mechanical model for the constitutive description.

It can be seen in the above relationships that $\bar{C}_r$ and $\bar{a}_r$ $(r = 0, 1, \ldots, n)$ should be positive due to the non-negative property of both the stored and dissipated energy. Although, in general, the variation of each $\bar{C}_r$ and $\bar{a}_r$ caused by damage can be different because of the complexity of internal structure and damage mechanism, it is assumed here that $\bar{C}_r$ and $\bar{a}_r$ $(r = 0, 1, \ldots, n)$ undergo the same damage in the sense that damage is defined as a reduction of load-carrying area (Lemaitre, 1984). Suppose ψ is a material integrity parameter that measures the macroscopic effect of damage, and assuming μ, C_r and a_r are respectively the $\bar{\mu}_r$, $\bar{C}_r$ and $\bar{a}_r$ in the undamaged and non-hardening state, it is reasonable to define

$$\bar{G} = \psi G(T), \qquad \bar{C}_r = \psi C_r(T), \qquad \bar{a}_r = \psi f a_r(T), \tag{7}$$

where f is a hardening function that is closely related to the internal structure of the material, its inelastic deformation history, residual microstress fields and deformation rate. The reduction of load-carrying area due to damage is not involved in f and its evolution.

Since a complete description of damage may involve anisotropic damage and a tensorial integrity parameter (Chern et al., 1992), a scalar damage parameter is introduced here to avoid complexity. Keeping in mind the relationships in Eqs. (5) and (7), the differential of Eq. (2) gives

$$\mathrm{d}\mathbf{Q}^{(r)} = \psi C_r(T)\,\mathrm{d}\mathbf{e}^{\mathrm{i}} - \alpha_r \mathbf{Q}^{(r)}\,\mathrm{d}z + \frac{\mathrm{d}\psi}{\psi}\mathbf{Q}^{(r)} + \frac{C_r'}{C_r}\mathbf{Q}^{(r)}\,\mathrm{d}T, \tag{8}$$

where

$$\alpha_r = \frac{C_r(T)}{a_r(T)}, \qquad \mathrm{d}z = \frac{\mathrm{d}\zeta}{f}, \qquad C_r' = \frac{\mathrm{d}C_r}{\mathrm{d}T}, \tag{9}$$

and T is temperature.

On the other hand, the elastic deviatoric response can be expressed as (Fig. 1),

$$\mathbf{s} = 2\bar{G}(T)(\mathbf{e} - \mathbf{e}^{\mathrm{i}}) = 2\psi G(T)(\mathbf{e} - \mathbf{e}^{\mathrm{i}}), \tag{10}$$

which leads to the following differential expression:

$$\mathrm{d}\mathbf{s} = 2\psi G(\mathrm{d}\mathbf{e} - \mathrm{d}\mathbf{e}^{\mathrm{i}}) + \frac{\mathrm{d}\psi}{\psi}\mathbf{s} + \frac{G'}{G}\mathbf{s}\,\mathrm{d}T. \tag{11}$$

The volumetric response is assumed to be elastic and described with

$$\sigma_{kk} = 3\bar{K}(\varepsilon_{kk} - 3\alpha(T)(T - T_0)) = 3\psi K(T)(\varepsilon_{kk} - 3\alpha(T)(T - T_0)), \tag{12}$$

where σ_{kk} and ε_{kk} are the volumetric stress and strain, K and α are the volumetric elastic modulus and the linear thermal expansion coefficient, respectively. The differential form of Eq. (12) is

$$\mathrm{d}\sigma_{kk} = 3\psi K\,\mathrm{d}\varepsilon_{kk} + \frac{\mathrm{d}\psi}{\psi}\sigma_{kk} + \left(\frac{K'}{K}\sigma_{kk} - 9\psi K\alpha'(T - T_0) - 9\psi K\alpha\right)\mathrm{d}T, \tag{13}$$

where $K' = \frac{\mathrm{d}K}{\mathrm{d}T}$, $\alpha' = \frac{\mathrm{d}\alpha}{\mathrm{d}T}$.

As was discussed above, the constitutive behavior of the materials subjected to thermomechanical loading incorporating fast heating may involve many influencing factors. Among them, the effect of plastic deformation, the effect of LTI and recrystallization on the hardening and damage may be dominant and will be mainly considered in this work.

4.2. Hardening function f and its evolution

The hardening of materials subjected to thermomechanical loading incorporating fast heating is related to the plastic deformation, the effect of LTI and recrystallization. It has been shown that high heating-rate can induce remarkable local residual stress due to the substantial heterogeneity of materials (Peng et al., 2003), which may lead to the hardening of the materials; on the other hand, recrystallization can eliminate the deformed microstructure and the corresponding hardening of materials. Taking into account of the effect

of inelastic deformation, LTI and recrystallization, the hardening function f can be expressed in the following simple form:

$$f = (1-\omega)f_1(z,\dot{T}) + \omega f_2, \tag{14}$$

where ω is the volume fraction of the recrystallized part of the material, f_2 corresponds to the hardening state of the material after recrystallization. If the original material is of recrystallization state and non-hardening state is achieved after recrystallization, one has $f_2 = 1$. If, in general, the original state of the material ready for use is different from that after recrystallization, then f_2 may be different from that corresponds to the initial state of hardening. $f_1(z,\dot{T})$ corresponds to the hardening induced by both plastic deformation and heating-rate, its evolution can be expressed as

$$\mathrm{d}f_1 = \beta_1(b(\dot{T}) - f_1)\,\mathrm{d}z, \tag{15}$$

where β_1 describes the rate for f_1 to approach $b(\dot{T})$, the saturated value of hardening. $b(\dot{T})$ is assumed to take the following linear form for simplicity:

$$b(\dot{T}) = b_0 + \gamma_1\dot{T}. \tag{16}$$

Recrystallization proceeds through the nucleation and growth of new grains. Recrystallization under isothermal condition can be described with Johnson–Mehl's relationship (Hassen, 1978), which was obtained under the following assumptions: arbitrary nucleation, constant nucleation and growth rates, negligible nucleation time compared with growth time. In the case of fast heating, the description of recrystallization should take into account the change of temperature in addition to the above four assumptions (Liu et al., 1996). Assuming the material with initial temperature T_0 is heated with a constant heating-rate k, the temperature T at moment t can be calculated with

$$T = T_0(1+kt), \tag{17}$$

where k denotes a constant heating-rate.

The nucleation and the growth rates of new grains can be described respectively with (Liu et al., 1996)

$$N = N_0 \mathrm{e}^{-\frac{Q_\mathrm{N}}{RT_0(1+kt)}} \quad \text{and} \quad G = G_0 \mathrm{e}^{-\frac{Q_\mathrm{G}}{RT_0(1+kt)}}, \tag{18}$$

where N_0 and G_0 are material constants, and Q_N and Q_G are the activation energy of nucleation and that of growth, respectively, which are, in general, related to existing plastic strain and applied stress. From Eqs. (17) and (18) and assuming that all grains are spherical, the volume fraction of recrystallization ω can be derived as (Liu et al., 1996)

$$\omega(\xi) = 1 - \exp\left[-\frac{S_2}{k^4}\int_0^{\xi} F(\xi')\mathrm{e}^{-\frac{S_3}{\xi'+\xi_0}}\,\mathrm{d}\xi'\right], \tag{19}$$

where

$$\xi = \frac{RT_0}{Q_\mathrm{G}}kt, \qquad \xi_0 = \frac{RT_0}{Q_\mathrm{G}},$$
$$S_2 = \frac{4\pi}{3}\left(\frac{Q_\mathrm{G}}{RT_0}\right)^4 G_0^3 N_0, \qquad S_3 = \frac{Q_\mathrm{N}}{Q_\mathrm{G}}, \qquad F(\xi') = \left[\int_0^{\xi'} \mathrm{e}^{-\frac{1}{\xi''+\xi_0}}\,\mathrm{d}\xi''\right]^3. \tag{20}$$

4.3. Damage D and its evolution

For simplicity, the macroscopic damage is assumed to be isotropic so that the integrity parameter ψ can be expressed as

$$\psi = 1 - D, \tag{21}$$

where

$$D = D_\mathrm{d} + D_{\dot{T}}. \tag{22}$$

D_d denotes the damage caused by inelastic deformation, for which the following assumptions are adopted: (1) damage may occur at the onset of inelastic deformation at an extremely low rate but accelerates as inelastic deformation develops, (2) the evolution of damage is related to the equivalent value of current state of effective stress $\bar{\sigma}_e$ and damage D, i.e.,

$$dD_d = g(D, \dot{T})(\bar{\sigma}_e)^{\beta_2} dz, \tag{23}$$

where

$$\bar{\sigma}_e = \sqrt{\frac{3}{2}\bar{\mathbf{s}} : \bar{\mathbf{s}}} \quad \text{with } \bar{\mathbf{s}} = \bar{\boldsymbol{\sigma}} - \frac{1}{3}\mathrm{tr}(\bar{\boldsymbol{\sigma}})\mathbf{I}_2, \tag{24}$$

$$\bar{\boldsymbol{\sigma}} = \frac{\boldsymbol{\sigma}}{\psi} = \frac{\boldsymbol{\sigma}}{1-D} \tag{25}$$

and $\mathbf{I}_2$ is the identity tensor of rank two.

$D_{\dot{T}}$ is related to the damage caused by LTI. It is known that the local residual stress related to LTI increases with the increase of $\dot{T}$, the following linear relationship is adopted for simplicity:

$$dD_{\dot{T}} = \gamma_2 \langle d\dot{T} \rangle, \tag{26}$$

where

$$\langle d\dot{T} \rangle = \begin{cases} d\dot{T}, & d\dot{T} > 0 \\ 0, & d\dot{T} \leqslant 0. \end{cases} \tag{27}$$

The combination of Eqs. (22), (23) and (26) yields the following evolution of damage:

$$dD = g(D, \dot{T})(\bar{\sigma}_e)^{\beta_2} dz + \gamma_2 \langle d\dot{T} \rangle. \tag{28}$$

5. Simulation and verification

5.1. Identification of the material constants

The elastoplastic behavior of LY12 subjected to thermomechanical loading incorporating fast heating is to be analyzed with the proposed model. For simplicity, the dependence of plasticity properties on temperature is considered with

$$C_r(T) = C_r^0 \theta(T) \quad (r = 1, 2, 3), \tag{29}$$

where C_r^0 is the magnitude of $C_r(T)$ at room temperature, and $\theta(T)$ is a temperature-dependent coefficient. It can be found that $\theta(T)$ is proportional to the rupture strength of a material, and can be determined using the variation of rupture strength against temperature. For LY12, it can be approximately determined as

$$\theta(T) = \begin{cases} 1 - 5.884 * 10^{-4}(T - T_0), & 20\,^\circ\mathrm{C} \leqslant T \leqslant 210\,^\circ\mathrm{C}, \\ 2.144 - 8.262 * 10^{-3}(T - T_0) + 8.692 * 10^{-6}(T - T_0)^2, & 210\,^\circ\mathrm{C} \leqslant T \leqslant 470\,^\circ\mathrm{C}, \end{cases} \tag{30}$$

where T_0 denotes room temperature and $T_0 = 20\,^\circ\mathrm{C}$ (or 293 K) is prescribed in computation. Fig. 9 shows the variation of $\theta(T)$ against T at sufficiently low heating-rate, and it can be seen that Eq. (30) can well describe the experimental results in the interested range of temperature.

It is known that the elastic properties of material are also affected by temperature, which are approximately assumed to follow the same rule as $C_r(T)$ for simplicity and without inducing remarkable error to the computed results, i.e.,

$$G(T) = G^0 \theta(T), \qquad K(T) = K^0 \theta(T), \tag{31}$$

where G^0 and K^0 are the elastic shear and volumetric moduli at room temperature, respectively.

It should be mentioned that for a phenomenological description, one usually uses a limited number of branches consisting of $\bar{C}_r$ and $\bar{a}_r$ $(r = 1, 2, \ldots, n)$ (see Fig. 1) to describe macroscopically and averagely the

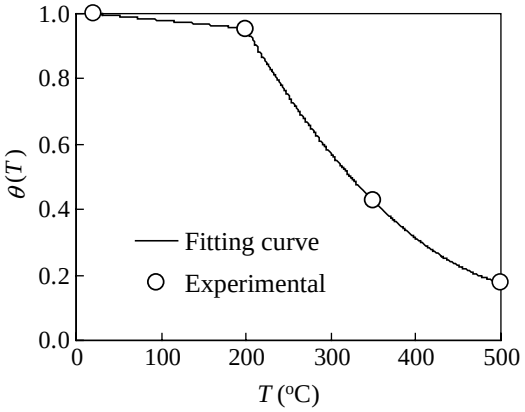

Fig. 9. The variation of θ against T (at sufficiently low heating-rate).

inelastic constitutive behavior of a material. In this work, $n = 3$ is adopted considering both accuracy and efficiency.

The material parameters and constants involved in this model can be classified into six groups and identified with the following approach:

(a) Elastic constants G^0 and K^0 can be determined with Young's Modulus E^0 and Poisson's ratio v obtained with a tensile testing of the elastic behavior of a material. The thermal expansion coefficient of LY12 can be found in the corresponding material handbook.
(b) Plastic constants: C_r^0 and α_r $(r = 1, 2, 3)$ as well as the hardening parameter b_0 and β_1 can be determined with an experimental σ–ε^{p} curve at room temperature with a non-linear curve fitting code.
(c) The temperature dependence $\theta(T)$ can be determined with the experimental rupture strength at different temperature and normal heating-rate.
(d) The parameter f_2 is related to the hardening state of the recrystallized material and can be determined with the ratio of the strengths of initial and recrystallized states of the material. The parameters related to recrystallization, ξ_0, S_2 and S_3 (Eqs. (19) and (20)) can be phenomenologically determined with the thermomechanical loading histories and the effect of recrystallization on the hardening/softening of the material. For example, given a set of thermomechanical loading histories, the hardening state f_1 before recrystallization and f after recrystallization for each case can be obtained, and the corresponding ω can be determined with Eq. (14). Then making use of Eqs. (19) and (20) as well as a curve-fitting code, the constants ξ_0, S_2 and S_3 can be identified.
(e) Damage parameters, β_2 and g (in this work, $g(D, \dot{T})$ is chosen as a constant g for simplicity), can be determined with experimental damage data, which can be phenomenologically obtained from the unloading slope on an experimental σ–ε curve at room temperature.
(f) The parameters related to the effect of heating-rate on the recovery of hardening and damage, γ_1 and γ_2, can be determined respectively with the differences in hardening and damage corresponding to different heating-rate.

The material constants identified are listed in Table 2.

5.2. Computation approach

Integrating Eq. (8) over the time interval t to $t + \Delta t$ leads to the following incremental expression:

$$\Delta \mathbf{Q}^{(r)} = \psi k_r C_r(T) \Delta \mathbf{e}^{\mathrm{i}} - k_r \left(\alpha_r \Delta z - \frac{\Delta \psi}{\psi} - \frac{\theta'(T)}{\theta(T)} \Delta T \right) \mathbf{Q}^{(r)}. \tag{32}$$

Table 2
Material constants

Elastic and thermal constants			Plastic constants					
G^0/GPa	E^0/GPa	α	C_1^0/GPa	C_2^0/GPa	C_3^0/GPa	α_1	α_2	α_3
29	75	22.5E−6	6260	28	4.4	25,000	410	52

Recrystallization				Hardening constants			Damage constants		
ξ_0	S_2/s^4	S_3	f_2	b_0	β_1	γ_1/(s/ °C)	g	β_2	γ_2/(s/°C)
2.0	5.0E−7	2.0	0.6	1.2	20	1.0E−4	1.0E−7	1.0	1.0E−4

Substituting Eq. (32) into the incremental form of Eq. (1) gives

$$\Delta \mathbf{s} = \sum_{r=1}^{n} \Delta \mathbf{Q}^{(r)} = A\Delta \mathbf{e}^{\mathrm{i}} + \mathbf{B}\Delta z + \mathbf{C}\Delta\psi + \mathbf{D}\Delta T, \tag{33}$$

where

$$A = \psi \sum_{r=1}^{n} k_r C_r(T), \qquad \mathbf{B} = -\sum_{r=1}^{n} k_r \alpha_r \mathbf{Q}^{(r)}, \qquad \mathbf{C} = \frac{1}{\psi}\sum_{r=1}^{n} k_r \mathbf{Q}^{(r)}, \qquad \mathbf{D} = \frac{\theta'(T)}{\theta(T)}\sum_{r=1}^{n} k_r \mathbf{Q}^{(r)}, \tag{34}$$

$$k_r = \frac{1 - \mathrm{e}^{-\Delta\bar{z}}}{\Delta\bar{z}}, \qquad \Delta\bar{z} = \alpha_r \Delta z - \frac{\Delta\psi}{\psi} - \frac{\theta'(T)}{\theta(T)}\Delta T. \tag{35}$$

The simulation can be carried out with an incremental approach. For readers to assemble the proposed model for code implementation and application more easily, the numerical approach for the case of a constant heating-rate and uniaxial tensile stressing is briefly introduced as follows:

Suppose the analysis for the nth increment of loading has been finished and t_n, z_n, T_n, $\theta(T_n)$, ψ_n, C_r, $Q_n^{(r)}$ $(r = 1,2,3)$, $f(z_n)$, ω_n, σ_n and ε_n have been obtained. Given the $(n+1)$th increment Δt_{n+1}, ΔT_{n+1} and $\Delta\sigma_{n+1}$, one can obtain $\dot{T}_{n+1}$, $\Delta\psi_{n+1}$ with Eqs. (23), (26) and (27), $\Delta \mathrm{e}^{\mathrm{p}}$ by combining of Eqs. (9) with (11), $\Delta\varepsilon$ with Eqs. (11) and (13), Δz_{n+1} with Eqs. (6) and $(9)_2$, $\Delta\omega_{n+1}$ with Eqs. (19) and (20), $f(z_{n+1})$ with Eqs. (16), (15) and (14), respectively. Then by superimposing the increments onto the corresponding results after the nth increment of loading, one obtains t_{n+1}, z_{n+1}, T_{n+1}, $\theta(T_{n+1})$, ψ_{n+1}, C_r and $Q_{n+1}^{(r)}$ $(r = 1,2,3)$, ω_{n+1}, σ_{n+1} and ε_{n+1}, and then starts for the neat increment of loading.

5.3. Simulation and verification

The effect of heating-rate history on the rupture strength of LY12 is analyzed and shown in Fig. 10. The material is heated at constant heating-rates 200, 650 and 1100 K/s to the final working temperatures, 200,

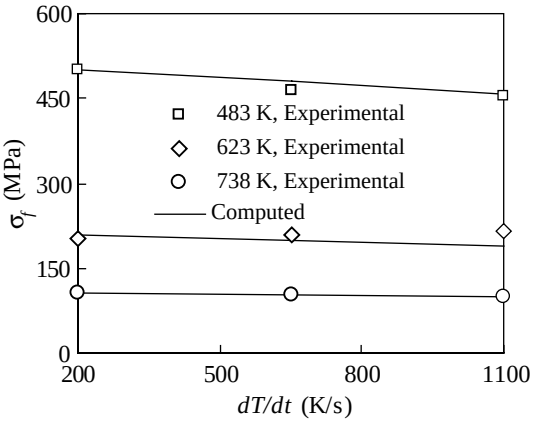

Fig. 10. The effect of heating-rate on σ_f (tension at elevated temperature).

350 and 465 °C (or 483, 623 and 738 K), respectively, the temperatures are kept unchanged for 0.5 s, followed by stretching the material until fracture. The computation is controlled by stress, temperature and time, and the failure is defined when instability, i.e., $d\sigma/d\varepsilon \to 0$ occurs during computation. It can be seen in Fig. 10 that the rupture strength, σ_f, decreases with the increase of either heating-rate or working temperature. The comparison between the computed and the experimental results shows that the proposed model can satisfactorily describe the effect of heating-rate history on the rupture strength of LY12.

Fig. 11 also shows the effect of heating-rate history on the rupture strength of LY12, where the material is heated at constant heating-rates 200, 650 and 1100 K/s, respectively, to 210 °C (or 483 K), then it is cooled

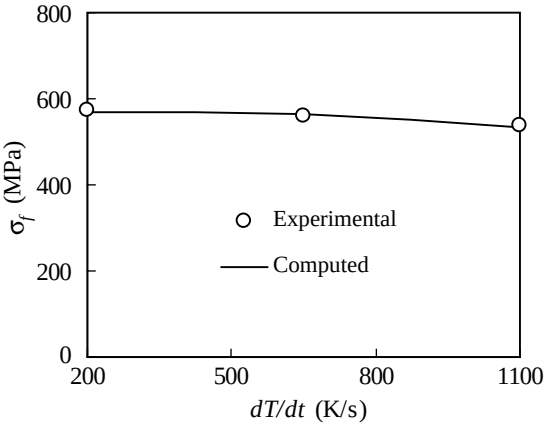

Fig. 11. The effect of heating-rate on σ_f (tension at cooled state).

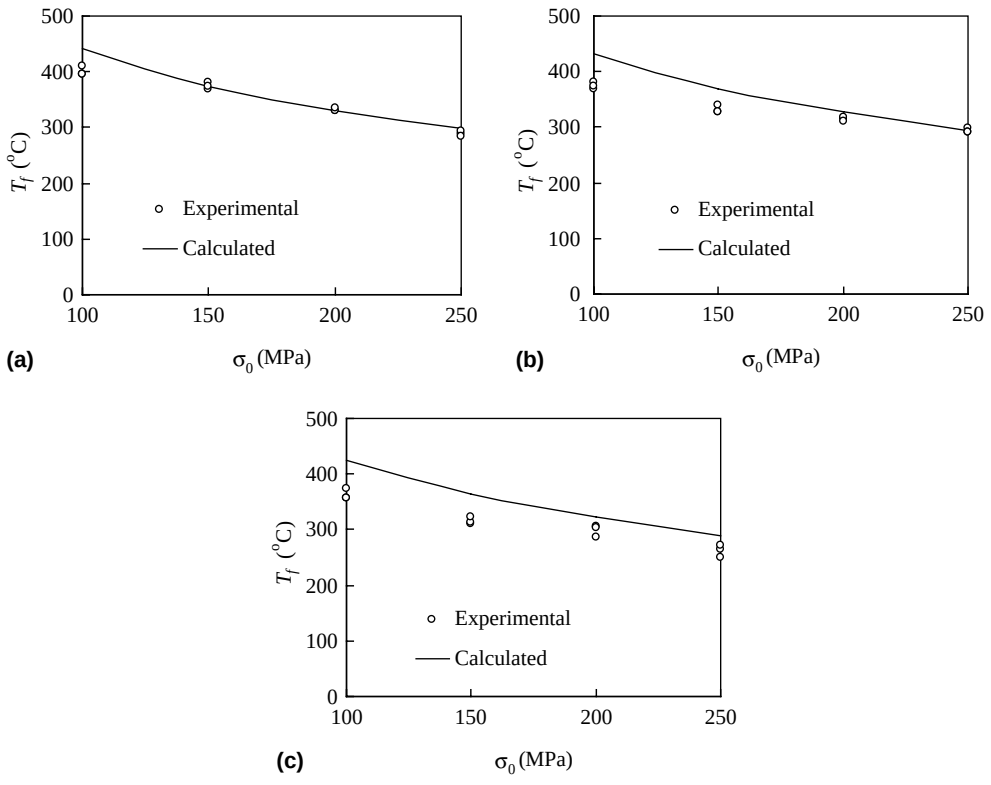

Fig. 12. Failure temperature T_f of preloaded LY12 heated at different heating-rate. (a) 200 K/s, (b) 600 K/s and (c) 1000 K/s.

naturally to room temperature, followed by tension to fracture. It can be seen that, although the maximum temperature is moderate, the effect of heating-rate history on the strength of the material can be observed distinctly, which decreases with the increase of heating-rate. The computed result is in satisfactory agreement with the experimental result.

The computed failure temperatures of the LY12 preloaded with different levels of stress are analyzed and shown in Fig. 12, where all the experimental data are also given for both comparison and showing experimental scatter. For each case the computation contains two steps: stretching the material to a prescribed stress, maintaining the preloaded stress unchanged while heating the material at a prescribed heating-rate until the failure of the material. Four levels of preloaded stress, 100, 150, 200 and 250 MPa, are prescribed, for each of which three different heating-rates, 200, 600 and 1000 K/s, are assigned. Since the computation process is stress-controlled, the failure temperature, T_f, can be defined as that at which instability occurs to the computation. It can be seen that the model can well describe the tendency of the effect of preloaded stress on failure temperature, but over predicts the failure temperature at higher heating rate. The error between the computational and the experimental results the can mainly be attributed to the following two reasons. (a) Although it is defined that the failure temperature is the temperature at which the specimen can no longer bear the prescribed preloaded stress, the exact determination of failure temperature is still difficult and may involve marked error. (b) The reduction of load-carrying area that exists in experiment is not taken into account in computation. In other words, the experiment is controlled by nominal stress (or load), and the actual tensile stress in a specimen should increase due to the reduction of load-carrying area provided the applied tensile traction is constant, which can partly account for the lower failure temperature in experiment.

6. Conclusions and discussion

The effect of heating-rate and its history on the mechanical behavior of aluminum alloy LY12 was experimentally investigated. It was found that the material experiencing histories of higher heating-rate possesses lower rupture strength, and the preloaded material will fail at a lower temperature when it is heated at a higher heating-rate. The SEM metallographical observation shows more defects in the material undergoing higher heating-rate histories. Analysis shows that the effect of heating-rate involves many factors such as hardening, recrystallization, damage, etc. A constitutive model was proposed for the material subjected to thermomechanical loading incorporating fast-heating, where the effect of heating-rate is introduced into hardening, damage with the concept of local thermal inconsistency and into recrystallization. The constitutive responses of LY12, subjected to thermomechanical loading incorporating fast-heating, were analyzed and compared with the experimental results. The satisfactory agreement between the computational and experimental results demonstrates the validity of the proposed model.

References

Chen, Y., 1997. Progress in structural mechanics in the Academy of Engineering Physics of China. In: Zhuang, F. et al. (Eds.), Modern Mechanics and Progresses in Science and Technology. Tsinghua University Press, Beijing, pp. 329–335.

Chen, Y., Li, S., 1992. Buckling failure of the axially pre-compressed cylindrical shell irradiated by CW CO2 laser beam. AIAA, 92–3231.

Chen, H. et al., 1992. Thermomechanical response of Al plates under tension to CW CO2 laser radiation. High Power Laser Part. Beams 4 (1), 141–147.

Chen, Y., Li, G., Zhang, J., 1995. Transient fatigue of aluminum plate in tension and irradiated by CW CO2 laser beam. High Power Laser Part. Beams 7 (2), 245–251.

Chen, B. et al., 2001. An experimental investigation to the effect of heating rate on the failure of pre-load H62 brass. Acta Metall. Sinica 37 (12), 1256–1260.

Chern, J.C., Yang, H.J., Chen, H.W., 1992. Behavior of steel fiber reinforced concrete in multiaxial loading. ACI Mater. J. 89, 32–40.

Fan, J., Peng, X., 1991. A physically based constitutive description for nonproportional cyclic plasticity. J. Eng. Mater. Tech. 113, 254–262.

Han, M., Liu, Z., Liu, Y., 1999. An experimental study on the mechanical behavior of A3 steel under rapid heating. Explosion Impact 19 (1), 20–26.

Hassen, P., 1978. Physical Metallurgy. Cambridge University Press, London.

Lemaitre, J., 1984. How to use damage mechanics. Nucl. Eng. Des. 80, 233–245.

Li, S., Chen, Y., 1994. Failure of shell subjected to internal pressure and irradiated by CW CO2 laser beam. AIAA, 94–2461.

Liu, Z., Han, M., Sun, C., Wang, R., 1995. Inelastic thermo-softening of metals under rapid heating. Acta Metall. Sinica 31 (7), B329–B335.

Liu, Z., Feng, Z., et al., 1996. Studies of thermo-softening of three alloys under short-time elevated temperature. Explosion Impact 16 (2), 98–104.

Peng, X., Ponter, A.R.S., 1994. A constitutive law for a class of two-phase materials with experimental verification. Int. J. Solids Struct. 31, 1099–1111.

Peng, X., Meyer, C., Fang, L., 1997. A thermomechanically consistent continuum damage model for concrete materials. J. Eng. Mech., ASCE 123, 60–69.

Peng, X. et al., 2003. Investigations to the effect of heating-rate on the mechanical properties of aluminum alloy LY12. Int. J. Solids Struct. 40 (26), 7385–7397.

Wang, C., Huang, C., Sun, Y., Duan, Z., 1995. Influence of heating rate and strain rate on tensile strength of 30CrMnSi. Acta Metall. Sinica 31 (10), A475–A478.